Int J Adv Manuf Technol (2018) 98:129–141
DOI 10.1007/s00170-017-0542-4

ORIGINAL ARTICLE

Determination of a coupling equation for milling parameters based on optimal cutting temperature

Jing Sheng [1,2] · **Yi-Jui Chiu** [1,2] · **Bing-Jing Lin** [2]

Received: 7 December 2016 / Accepted: 9 May 2017 / Published online: 27 May 2017

Abstract The optimization of cutting parameters has a great concern in the field of manufacturing process, especially the relationships among cutting parameters, with the study aiming at exploring a coupling equation to cutting parameters based on the optimal cutting temperature in the milling process of precipitation-hardening stainless steel with cemented carbide inserts. Initially, the association among the ratios of cutting tool wear of the machined surface, the cutting speed, and temperature was respectively investigated, with the ratio also used as an evaluating level of tool wear. Afterwards, the effects of the work hardening layer depth and the work hardening degree on the cutting speed and temperature were discussed in order to evaluate the machined surface quality. The results indicate that while the minimum tool wear occurred, the tool tip temperature at the cutting zone stayed the same with the minimum degree of work hardening appearing, which was defined as the optimal cutting temperature. An empirical formula for the cutting temperature and cutting parameters is explored using regression orthogonal experiment design, and then combined with optimum temperature. As a result, a coupling equation to cutting parameters is determined. Meanwhile, the mechanism of the minimal cutter wear is analyzed in accordance with the characteristics of cutting tool wear under several different machining conditions. The coupling equation could be put into an optimization model as a constraint. The results of this research would be beneficial to application of cooling liquids and cooling method to achieve cleaner production as well as the construction of a cutting database of metal materials.

Keywords Cutting tool wear · Cutting temperature · Coupling equation for milling parameters · Orthogonal experiments · Cutting parameter optimization equation

Nomenclature

T	Temperature of a point in cutting zone.
T	Time parameter.
$\frac{\partial T}{\partial x}, \frac{\partial T}{\partial x}, \frac{\partial T}{\partial x}$	Temperature gradient in the x-direction, y-direction, and z-direction.
λ	Heat conduction coefficient of material.
ρ	Material density.
C	Heat capacity.
w_x, w_y, w_z	Velocity components of a moving heat source at x-direction, y-direction, and z-direction.
q^*	Heat generation rate per unit volume.
T_l	Service life of cutter.
C_T	Coefficient of tool service life relating to cutter, workpiece, and cutting condition.
v, f, a	Cutting speed, feed rate, and the cutting depth.
m, n, p	index of $c$utting speed, the feed rate, and the cut depth on the tool service life.
θ	Average temperature of cutting zone.
C_θ	Correction coefficient of cutting temperature.
a_e, a_p, f_z	Radial cutting depth, axial cutting depth, and feed rate per tooth.

✉ Jing Sheng
shengqqqqjing@163.com; shengjing@xmut.edu.cn

[1] Fujian Collaborative innovation center for R&D of coach and special vehicle, Xiamen University of Technology, Xiamen, Fujian, People's Republic of China

[2] School of Mechanical and Automotive Engineering, Xiamen University of Technology, Xiamen, Fujian, People's Republic of China

C_e, C_p, C_f,C_v	Exponents of radial cutting depth, axial cutting depth, feed rate, and cutting speed on cutting temperature.
y, x_1, x_2, x_3, x_4	Common logarithm of cutting temperature, radial cutting depth, axial cutting depth, feed rate, and cutting speed.
b_0, b_1, b_2, b_3, b_4	Common logarithm of exponents of radial cutting depth, axial cutting depth, feed rate, and cutting speed on cutting temperature.
Z_1, Z_2, Z_3, Z_4	The orthogonal test code of cutting temperature, radial cutting depth, axial cutting depth, feed rate, and cutting speed.
θ_s	The highest temperature on the test surface.
ε	Radiation rate of the measuring surface.
σ	Stephen Boltzmann constant.
T_2	Absolute temperature on the test surface.
δ	Distance from cutting area to measuring surface.
DOF, SS, MS, F, P	Degree of freedom, stdev square, mean square, F statistic value, and significance F.
v_0	Cutting speed at optimum cutting temperature.
N_{Brs0}	Wear of the tool flank at the optimum cutting temperature.
c_1, c_2	Coefficients of feed rate on cutting speed and wear of the tool flank at optimum cutting temperature.
y_1, y_2	Exponents of feed rate on cutting speed and wear of the tool flank at optimum cutting temperature.
N_B	Tool flank wear amount.
L	Cutting route length.
B	Milling width.
N_{Brs}	Tool flank wear amount per 1000 cm^2 cutting surface area.

1 Introduction

Irrational cutting parameters can significantly influence the product processing quality and production costs, resulting in a considerable waste of energy. In using tools and cooling lubricants, it will inevitably produce consumption during the cutting process of metal parts. Also, its emission has a serious impact on the environment. Previous environmental studies on equipment used in component manufacturing (e.g., turning and milling) show that a large proportion of environmental impacts result from the electrical energy consumption [1]. Consequently, the cleaner production is becoming a popular industry trend.

In terms of parameter optimization, Bhushan et al. [2] suggested that experimental investigations should be conducted to analyze the effects of cutting speed, depth of cut, feed rate, and nose radius on power consumption. The response surface methodology was employed in the turning of 7075 aluminum alloy SiC composite. The results showed that power consumption was reduced and that tool life was increased when the optimized parameters mentioned above were adopted. Camposeco-Negrete et al. [3] mentioned that cutting energy consumption and surface roughness were considered as an optimization goal during the turning of AISI 6061 T6 under adverse conditions. An orthogonal array, the variance (ANOVA), and the ratio signal to noise (S/N) were used to analyze the effects of cutting parameters on the response variable. Regarding energy consumption, the feed rate was the most important factor, followed by depth of cut and the cutting speed. Yildiz [4] gave a solution to the optimal problem from machining parameters in multi-pass turning process by an evolutionary-based hybrid artificial bee colony algorithm (HABC). The findings showed that the HABC had high competitiveness compared with other published algorithms in the literature for getting the cutting optimization solution.

Tool wear can not only consume resources but also affect the processing quality and the energy consumption. Liu et al. [5] explored the predictive models for discussing the links between material removal rate and embodied energy, emissions, and environmental influence. Yusup et al. [6] pointed out that machining parameters related to tool wear as metal cutting can affect productivity, processing quality, and production costs. Consequently, the optimization of cutting parameters has been a hotspot issue. Besides, Pervaiz et al. [7] discussed the power consumption, tool wear, and surface roughness during the turning of titanium alloy Ti-6Al-4V with coated PVD and uncoated carbide inserts. Lower feed rate and cutting speed led to higher energy consumption. Compared with that in a humid environment, less energy was consumed in a dry environment with better results for flank wear. Bhattacharya et al. [8] studied the high-speed cutting at AISI 1045 with coated carbide inserts. The effects of cutting parameters on surface roughness of workpieces and power consumption were quantitatively analyzed using the Taguchi technique and the variance analysis method. The study results revealed that cutting speed had a remarkable effect on power consumption and surface roughness. Moussaoui et al. [9] presented a method for balancing transverse cutting force to reduce cutter wear in milling titanium alloy workpieces. The method improved cutting conditions and increased the productivity of rough machining. Lawal et al. [10] compared performances of three types of cutting fluids by obtaining the effects of cutting fluids in processing the AISI 4340 with coated carbide inserts using the Taguchi experimental method. They developed a mathematical model for cutting parameters by adopting regression analysis to estimate the flank wear, with experiments performed to confirm the regression equations based the optimized values. The results demonstrated that using two cutting fluids could improve

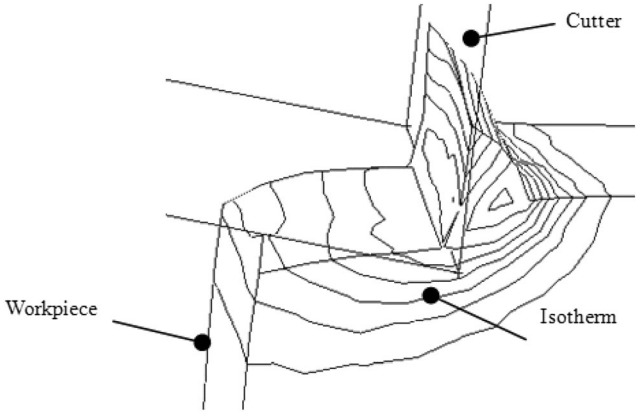

Fig. 1 The temperature field at the cutting zone

the machining condition. Muthusamy et al. [11] investigated wear characteristics and cutter life during the end milling of AISI304 with water-soluble coolant and nanoparticle-based coolant using a TiN-coated carbide insert. The research results indicated that the tool life increased as the cutting parameters decreased, and that the end-milling process with nanoparticle-based coolant showed a better performance than that with water-soluble coolant in terms of tool life. There is a severe thermos-mechanical coupling effect between cutting tools and workpieces during cutting process. Chetan et al. [12] found that the tool wear mechanisms involved were predicted under a variety of conditions during the turning of Ti alloy (Ti-6Al-4V), with their analytical mathematical model established. Park et al. [13] found that cutting tool wear at low temperature was more violent than that at high one. Cui et al. [14] found that periodically changing cutting thickness due to the saw-tooth formation greatly influenced the periodic variation of the cutting force, tool temperature, and tool stress. The actual change of the cutting thickness caused by a higher degree of cutting-speed-forming serrated chip resulted in greater mechanical and thermal impacts. Compared with the tool temperature, the cutting force had less effects on the tool stress when the cutting speed was correspondingly high. Bugdayci et al. [15] carried out the thermal analysis considering shearing and frictional heat generations in the primary and secondary zones. Prediction and experimental investigations were conducted to determine the basis of combination of the cobalt hard alloy milling Al-7050 concentration of the highest temperature and the hardness of the tool flank wear. The analysis clearly indicated that the cobalt concentration could significantly influence the tool flank wear of aluminum alloy Al-7050.

In order to control machined surface quality and cutting tool wear, Lin et al. [16] investigated the application of oils to water (OoW) as a cooling means in turning Ti-6Al-4V alloy aiming at discussing the influence of oils on water cooling. Compared with CAMQL, IOoW cooling with a proper quantity of water or EOoW cooling with an appropriate position led to smaller surface roughness and lower tool flank wear. The use of cutting fluids affecting sustainable manufacturing, Neto et al. [17] invented a tool-holder to implement cooling of cutting tool. Tool life, wear mechanisms, and temperatures were compared with cutting fluid, the internal cooling method, or dry cutting during cutting experiments. It was found that internal cooling can extend tool life. Luo et al. [18] researched the wear mechanism of coated insert during end-milling titanium alloy Ti-6Al-4V, with the result found that the wear behavior of the cutter gradually changed in the range at different cutting speeds.

Part of the investigations in the literature reviews showed the wear and damage mechanisms of the tool in isolation under a condition with ignorance of the internal factors inducing them (cutting force and cutting temperature) with the relationship among wear, tear, and cutting temperature less considered systematically. By contrast, in the result of cutting process optimization, one or more goals among the machining quality and tool wear were considered. How to coordinate the active control of tool wear with other goals is a key issue in the optimization of cutting process. Hao et al. [19] studied the tool wear mechanism in turning nickel-based alloy Inconel 718 with PVD-coated carbide tools, with an optimum cutting temperature proposed. At a certain temperature, tool wear could reach the minimum value. For a tool workpiece, the cutting conditions could be optimized to obtain the minimum tool wear in order for the cutting temperature could reach the optimum value. An ideal tool-wear-controlling method should provide a theoretical basis and an effective method for the proper selection of cutting parameters. Sheng [20] presented a method for the definition of the optimal cutting temperature in the dry turning of a kind of precipitation

Fig. 2 Metallographic structure (800×)

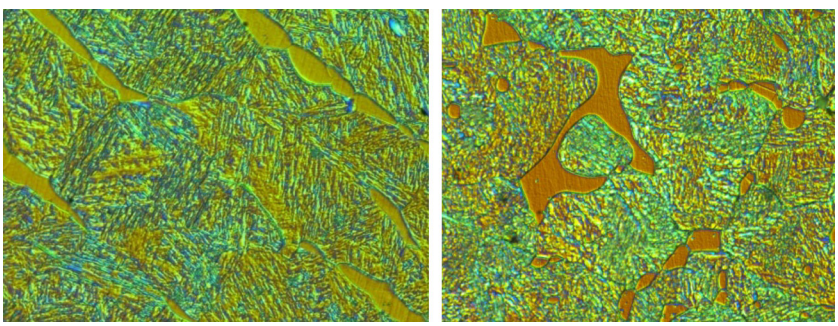

(a) Structure in one direction (b) Structure in the other direction

hardened with cemented carbide YT15 inserts. The relationship between tool wear value and cutting speed was observed under the condition at a constant feed rate, showing that optimal cutting temperatures in different conditions were the same. The tool wear mechanism was discussed under several conditions around at the optimum cutting temperature.

The above studies focus mainly on the expression between cutting parameters, machining quality, and tool wear, which is not accurate enough but very complicated, causing many problems in the optimization of cutting parameters. In fact, the optimization results of machining parameters depended mainly on an objective function and constraints composed of the expressions. However, in the constraint of a model, no efforts were made to establish the coupling equation based on either the minimum tool wear or workpiece surface quality.

In this work, an attempt was made to build an equation in contact with the cutting parameters based on the optimal cutting temperature during the milling of precipitation-hardening stainless steel using experimental methods. The optimization equation containing between a cutting speed, a feed rate, an optimal wear value, and a feed rate was studied in the case of a given radial and axial depth of cut.

2 Temperature field and cutter wear theory

2.1 Temperature field of cutting

The work is conducted at the deformation zone of both elastic and plastic deformation of metal cutting layer and friction between chips generating cutting heat. A heat conduction governing the equation of a three-dimensional unsteady temperature field in a rectangular coordinate system can be written as follows:

$$\rho C\frac{\partial T}{\partial t}=\lambda\left(\frac{\partial^2 T}{\partial x^2}+\frac{\partial^2 T}{\partial y^2}+\frac{\partial^2 T}{\partial z^2}\right)+\frac{\mathrm{d}\lambda}{\mathrm{d}T}\left[\left(\frac{\partial T}{\partial x}\right)^2+\left(\frac{\partial T}{\partial y}\right)^2+\left(\frac{\partial T}{\partial z}\right)^2\right]-\rho C\left(w_x\frac{\partial T}{\partial x}+w_y\frac{\partial T}{\partial y}+w_z\frac{\partial T}{\partial z}\right)+q^* \quad (1)$$

(a) Machining center

(b) Milling cutter

Fig. 3 Machining center and milling cutter

Table 1 Chemical composition of workpiece material

Alloy element	Cr	Mn	Ni	Mo	Al	Si
Percentage[%]	11.6	4.27	4.07	3.03	0.93	0.54

The temperature field in the cutting process is shown in Fig. 1.

2.2 Cutter wear

The occurrence of cutter wear can be found simultaneously both on the front cutter face and on the back cutter face. The wear mechanism usually includes adhesive, diffusion, abrasive particle, and oxidation. The relationship between the cutting parameters and cutter life T_1 can be expressed in Eq. 2:

$$T_1 = C_T/(V^m f^n a^p) \quad (2)$$

Equation 2 cannot well express the coupling relationship among cutting parameters, tool life, and cutting temperature. Additionally, the cutting parameters determined by this equation only explain the mechanical action resulting in a tool wear, but could not make an influence on the thermal effect clear.

3 Experimental procedure

The material used here is a kind of precipitation-hardening stainless steel, which has undergone the solid solution at 1050 °C, cold treatment at −78 °C, and aging at 520 °C. Its final alloy structure is composed of martensite, residual austenite, precipitated phase (NiAl), and a small amount of δ-ferrite as shown in Fig. 2. Figure 2a, b is about the metallographic structures in two vertical directions. Evident martensite and ferrite structures can be seen in the Fig. 2. The material has the hardness of 30–38 HRC and yield strength of 626 Mpa.

The experiment involving cutting temperature, work hardening capacity, and tool wear was employed in the investigation. The milling equipment machining center (KVC650 manufactured by Zigong Changzheng Machine Tools Co., Ltd.) is seen in Fig. 3a. The milling cutter is of cemented carbide YG8, with a diameter of 80 mm and tooth number

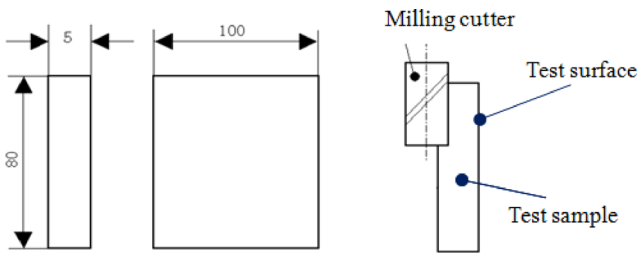

Fig. 4 Shape and dimension of the test sample

Table 2 The milling parameters and the levels of the cutting temperature experiment

Cutting parameter	Level 1	Level 2	Level 3
a_e (mm)	2.00	2.45	3.00
a_p (mm)	5.00	7.10	10.00
f (mm/min)	37.5	47.5	60.0
v (m/min)	23.6	29.5	37.3

3. Refering to Fig. 3b, dry milling, end milling, and up milling modes were adopted. The chemical composition of the workpiece material is shown in Table 1.

The testing instruments and equipment are as follows: an infrared thermograph (DB69780-P), a scanning electron microscope (Leo1450VP), a scanning electron microscope (SEM), a micro hardness tester (FM-700), an energy spectrum analyzer (THERMOL VANTAGE DSI), and a microscope (LYMPUSGX71).

3.1 The experiment of cutting temperature

The shape and dimension of the test sample can be seen in Fig. 4, with the process parameters and their levels of the cutting temperature experiment shown in Table 2.

Under the condition of constant cutting operation, the general form of the empirical formula of the cutting temperature can be expressed by Eq. 3,

$$\theta = C_\theta a_e^{C_e} a_p^{C_p} f^{C_f} v^{C_v} \tag{3}$$

With the usual logarithmic transformation, the data in Table 2 was changed into Table 3 and Eq. 3 is expressed as follows:

$$y = b_0 + b_1 x_1 + b_2 x_2 + b_3 x_3 + b_4 x_4 \tag{4}$$

where $y = \lg\theta$, $x_1 = \lg a_e$, $x_2 = \lg a_p$, $x_3 = \lg f$, $x_4 = \lg v$, $b_0 = lgC_\theta$, $b_1 = \lg C_e$, $b_2 = \lg C_p$, $b_3 = \lg C_f$, and $b_4 = \lg C_v$.

The regression orthogonal experiment design was adopted and an $L_9(3^4)$ orthogonal array was used to design the experiment. The transform formulas for the encodings of each factor level were expressed as follows,

$$Z_1 = (\lg a_e\text{-}0.39)/0.09 \tag{5}$$

Table 3 The milling parameters and the levels

Cutting parameter	Level 1	Level 2	Level 3
$\lg a_e$	0.30	0.39	0.48
$\lg a_p$	0.70	0.82	0.94
$\lg f$	1.60	1.69	1.78
$\lg v$	1.38	1.42	1.46

Table 4 Orthogonal experiment array at cutting temperature

Experiment no	Z_0	Z_1	Z_2	Z_3	Z_4	θ_m (°C)	$\lg\theta_m$
1	1	−1	−1	−1	−1	280.00	2.4472
2	1	−1	0	0	0	310.00	2.4914
3	1	−1	1	1	1	345.00	2.5378
4	1	0	−1	0	1	353.00	2.5478
5	1	0	0	1	−1	300.00	2.4771
6	1	0	1	−1	0	315.00	2.4983
7	1	1	−1	1	0	335.00	2.5250
8	1	1	0	−1	1	363.00	2.5599
9	1	1	1	0	−1	305.00	2.4843

$$Z_2 = (\lg a_p\text{-}0.85)/0.15 \tag{6}$$

$$Z_3 = (\lg f\text{-}1.68)/0.10 \tag{7}$$

$$Z_4 = (\lg v\text{-}1.47)/0.10 \tag{8}$$

Equation 4 is transformed into Eq.9.

$$y = b_0 + b_1 Z_1 + b_2 Z_2 + b_3 Z_3 + b_4 Z_4 \tag{9}$$

The orthogonal experiment array at the milling temperature was designed (Table 4); the temperature value on test surface was acquired from the infrared temperature graph (see Fig. 5); the temperature at cutting zone was obtained from the calculation of Formula (10).

$$\theta_m = \theta_s + \varepsilon\sigma T_2^4 \delta/\lambda \tag{10}$$

The milling temperature in the cutting region is shown in Table 4 by measuring and converting.

3.2 The experiment of work hardening capacity

Four different feed rates of 0.1, 0.15, 0.2, and 0.25 mm/tooth, depth of cut of constant 5 mm, width of cut of constant 5 mm,

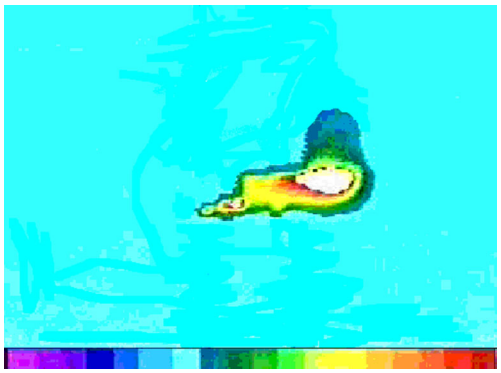

Fig. 5 Infrared temperature graph at the measured surface in milling

Table 5 The ratio of the cutter wear to the 1000 cm^2 cutting area.

Feed rate per tooth f_z (mm/tooth)	Cutting speed $v\ (m/min^{-1})$/ Wear value divided by cutting area $N_{\mathrm{Brs}}\left(\mathrm{mm}/\left(10^{-3}\cdot cm^2\right)\right)$						Machining temperature corresponding toN_{Brs0} (°C)
0.10	30/9.1	35/5.9	43/20	50/42	55/57	62/76	272
0.15	26/12	30/8.1	32/4.5	36/7.0	43/28	50/50	276
0.20	26/11	29/3.5	32/9.0	36/14	43/40	50/67	268
0.25	22/18	25/2.5	30/8.0	35/20	43/54	50/85	280

and six different cutting speeds with 20–60 m/min were employed in the milling experiment to explore the work hardening capacity.

3.3 The experiment of tool wear

The experimental procedure was carried out according to the following steps:

1. The 0.5 mm of wear value of the rake was considered as cutter blunting, with the test carried out at the normal wear stage of the cutter.
2. Feed rates were selected at 0.10, 0.15, 0.20, and 0.25 mm/tooth separately. Both the milling depth and the width of cut were fixed to constant 0.5 mm. Five different cutting speeds were adopted as well. The cutting route length L being reached, the wear value N_B of milling cutter could be measured using reading microscope when the cutter was cooled. Meanwhile, the machining temperature value was obtained by the method mentioned above.

4 Experiment data processing

4.1 The empirical formula at cutting temperature

The accuracy of the empirical formula at cutting temperature was tested by the analysis of variance of regression orthogonal experiment (see Table 6) and F test, an examination of the significance of each factor. The analysis of a significance level α = 0.1 (confidence level of 90%) was carried out. The F values of each factor exceeded $F_{0.1}$, and the regression error exceeded $F_{0.005}$. Therefore, the four factors are of significance with the level α = 0.1, and linear regression was of significance with the level α = 0.005.

4.2 The cutting parameter equation of cutting process optimization

Assuming that the optimal cutting speed is v_0 (optimum cutting speed) and the minimum ratio of wear of the cutting area is N_{Brs0} (minimum wear value),

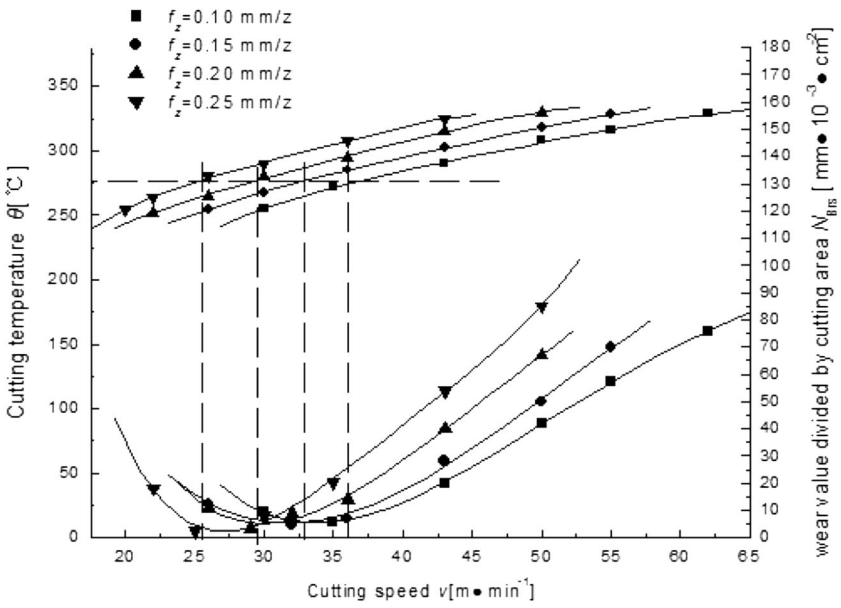

Fig. 6 The relationship among flank wear value, the machining temperature, and the cutting speed

Table 6 Analysis of variance of regression orthogonal experiment

Factor	DOF	SS	MS	F	P
Z_1	1	0.0086	0.0086	172	55.8 ($F_{0.1}$)
Z_2	1	0.0245	0.0245	490	55.8 ($F_{0.1}$)
Z_3	1	0.0041	0.0041	80	55.8 ($F_{0.1}$)
Z_4	1	0.0095	0.0095	190	55.8 ($F_{0.1}$)
Regression error	4	0.0467	0.0117	234	23.15 ($F_{0.005}$)
Error	4	0.0002	0.00005		
Total	8	0.0469			

the f_z-v_0 and f-N_{Brs0} relation equations [20] will be obtained.

$$v_0 = c_1/f^{y_1} \tag{11}$$

$$N_{\mathrm{Brs}_0} = c_2/f^{y_2} \tag{12}$$

Equations 11 and 12 are the equations of the optimized cutting parameters during milling (also called the maximum cutter durability equation). The cutting route of cutter would be the longest when these equations are defined.

4.3 The evaluation of tool wear

The evaluation of tool wear adopted the tool flank wear value per 1000 cm^2 cutting surface area, which were obtained from the equation below:

$$N_{\mathrm{Brs}} = \left(N_{\mathrm{B}} \times 10^5\right)/(L \times B) \quad \mathrm{mm}/\left(10^3 \times \mathrm{cm}^2\right) \tag{13}$$

5 Results and discussion

5.1 The relationship of the cutting tool wear and cutting parameters at optimal cutting temperature

The ratios (N_{Brs}) of the wear of the cutting area are shown in Table 5, and the cutting speeds, the ratio of the wear of the cutting area, and the corresponding machining temperature at various feed rates are in Fig. 6. It can be seen from the Fig. 6 that the machining temperature corresponding to the minimal value of N_{Brs0} at different feed rates is between 268–280 °C. When the mean value is taken, the optimal machining temperature for using the tool during workpiece milling is 275 °C.

The results show that the effects of cutting parameters on the machining temperature are the same as that for the tests of other materials; cutting speed has the greatest effect on the machining temperature, followed by width of cut, feed rate, and depth of cut.

Table 7 Coefficients and exponents in the equation for optimizing the cutting parameters of cutting process

x_1	c_1	x_2	c_2
0.069	29.475	0.714	1.241

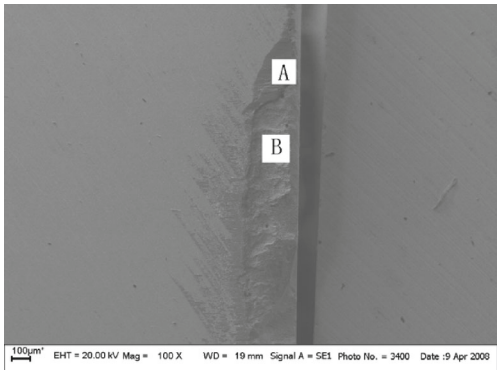

(a) Wear pattern of the wear cutter face at v=30m/min

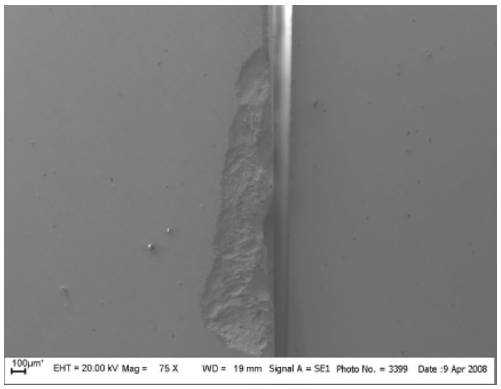

(b) Wear pattern of the wear cutter face at v=40m/min

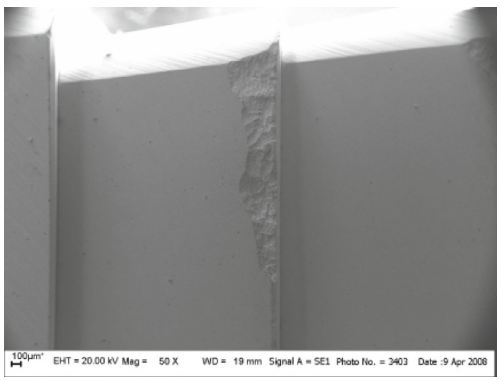

(c) Wear pattern of the wear cutter face at v=50m/min

Fig. 7 Wear patterns of the wear cutter face

5.2 The empirical formula of the cutting temperature

The empirical formula of the temperature at the cutting zone was obtained in regression orthogonal table (Table 4).

$$\theta = 57.78 a_{\mathrm{e}}^{0.1722} a_p^{0.0007} f^{0.0580} v^{0.3950} \tag{14}$$

Fig. 8 Energy spectrum analysis diagrams of the wear zones at wear cutter face

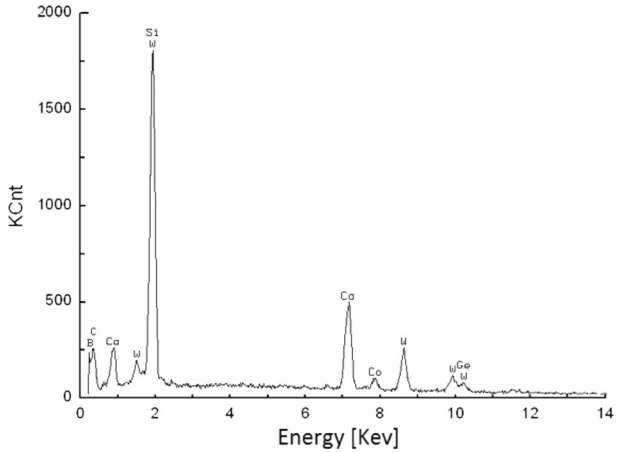

(a) Wear zone energy spectrum analysis of wear cutter face at v=30m/min

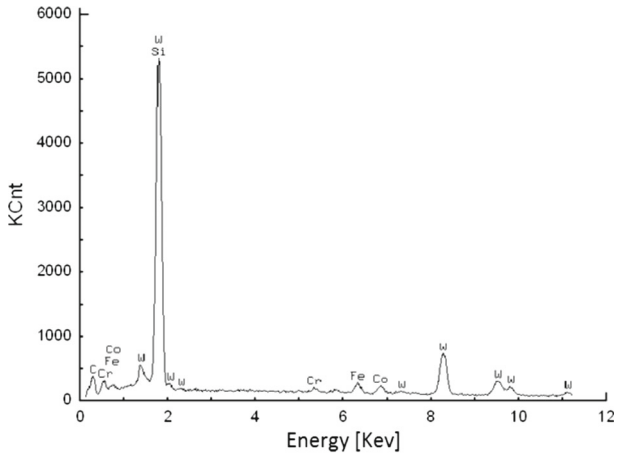

(b) Wear zone energy spectrum analysis of wear cutter face at v=40m/min

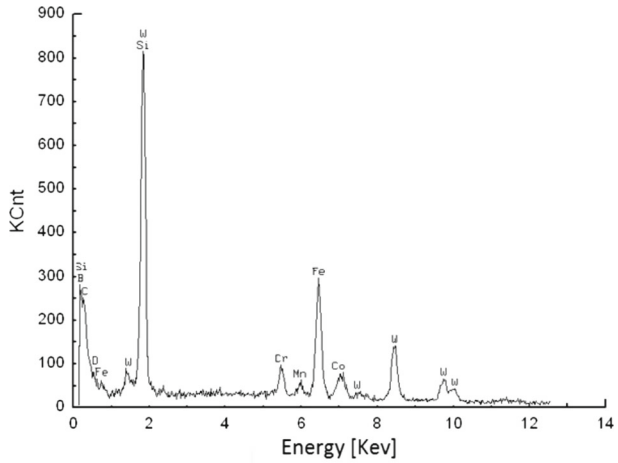

(c) Wear zone energy spectrum analysis of wear cutter face at v=50m/min

5.3 The analysis of the tool wear mechanisms

To study the relationship between the optimal cutting parameters and the machining temperature, tool wear patterns and the causes at a feed rate of f_z = 0.10-mm/tooth were discussed.

Fig. 7 **a**–**c** are the wear patterns of the wear milling cutter face at the milling speeds of 30, 40, and 50 m/min,

respectively. Figure 7 is the energy spectrum analysis diagram of the corresponding tool wear zones

A combination of Fig. 7 a–c (wear patterns of the wear cutter face) with Fig. 8a–c (energy spectrum analysis of the wear zone of cutter face) shows that the main elements at the tool wear zone of the cutter face are those in cemented carbide YT5 material such as Co and W. However, there are also elements and impurities from the workpiece such as Cr, Mn, and Fe. Some elements of the cutter material can also be found in milling chips. Besides, it can be found from the figures that when the milling speed is increased to 50 m/min, the cutter face mainly has the matrix elements. There are also obvious grooves on the cutter face, an indication that it is the abrasive particle wear. The wear is caused by the friction between the precipitated phase (NiAl) of workpiece and TiN with the high hardness in the phase and the cutter face.

The cutting speed being lower than about 35 m/min; the cutter failure is due mainly to the adhesive wear. While at a higher speed, its failure is due mainly to abrasive particle wear. With the increase of speed, the cutter wear is intensified. This illustrates that the optimal machining temperature is at the temperature zone corresponding to the occurrence of slight adhesive wear of the cutter.

It can be seen in Fig. 6 that when the cutting tool material is used for the cutter during workpiece milling at the feed rates of 0.10, 0.15, 0.20, and 0.25 mm/tooth, the corresponding optimal cutting speeds are 36, 33, 29, and 26 m/min, respectively, with the minimum values of ratio (N_{Brs0}) of the wear to the cutting area being 6.0, 5.2, 3.5, and 3.0 mm/($10^3 \times cm^2$). The equation for optimizing the cutting parameters of cutting process can be found by the unitary linear regression method (see Table 5).

5.4 The equations of the optimized cutting parameters

The data in Table 5 was processed, and the minimum tool wear value, optimal cutting speeds at optimal cutting temperature were obtained. According to Eqs. 11 and 12, the coefficients and exponents in the equation for optimizing the cutting parameters of machining process (see Table 7) were acquired with the help of regression processing.

The relationship between the minimum wear value and feed rate per tooth at the optimal machining temperature is shown in Fig. 9, and the relationship between optimum cutting speed and feed rate per tooth at the optimal machining temperature can be seen in Fig. 10.

5.5 The analysis of the work hardening capacity

Sample 1 was performed under the condition at the feed rate of $f = 0.1$ mm/tooth and cutting speed $v = 30$ m/min. The micro hardness trend of sample 1 is shown in Fig. 11a and SEM image of metallurgical structure of sample 1 in Fig. 11b. From sample 1, we can see that between 0.010 and

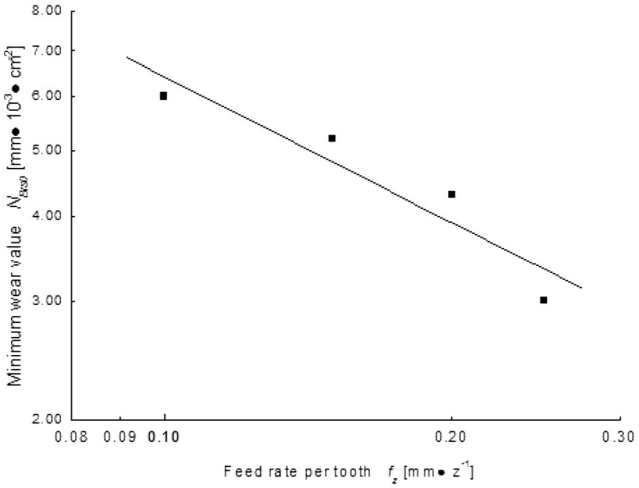

Fig. 9 The double logarithmic curve between minimum wear value and feed rate per tooth

0.035 mm of the depth underneath the surface, the micro hardness shows a steady decrease from 326 to 300 HV, basically close to the original structural hardness of 303 HV. The change of the micro-hardness values in sample 1 indicates that the depth of the hardening layer is about 0.035 mm, and that the degree of work hardening is about 7.5%. It shows an obvious zone of plastic deformation, 6 μm in depth underneath the surface which is normally called the amorphous layer. This is a thin residual layer caused by the rounded cutting edge radius in the cutting thickness, resulting in further elastic deformation of the machined surface that is subject to the rounded cutting edge compression and also the compression and the friction of the tool flank. The martensite and other structures on the plastically deformed layer of the subsurface are elongated and streamlined under the action of milling forces, thereby causing the crystal grains to be dislocated. Moreover, the materials with slight crystal boundary dislocation are subject to compression and friction forces.

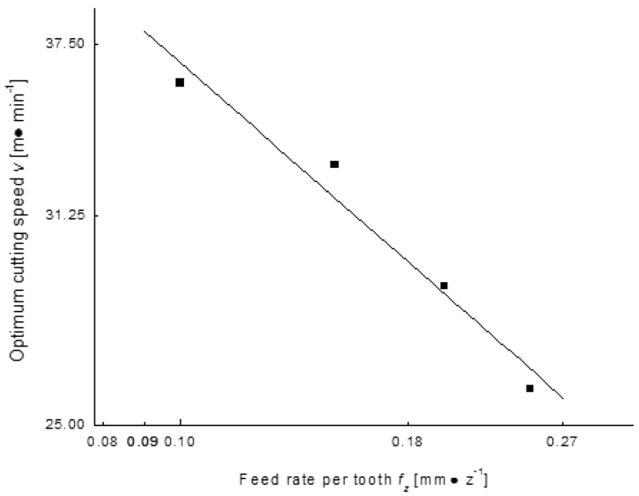

Fig. 10 The double logarithmic curve between optimum cutting speed and feed rate per tooth

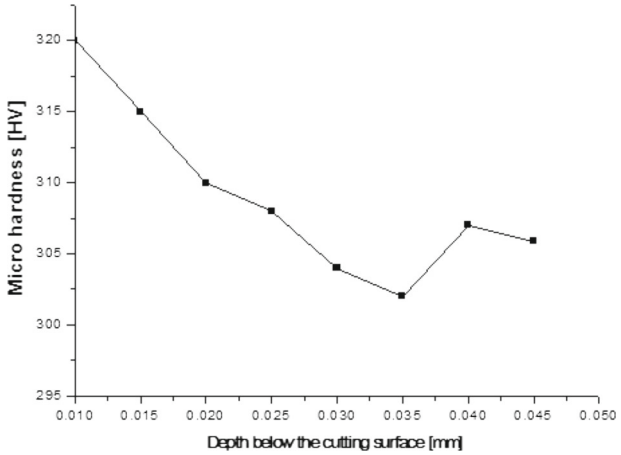

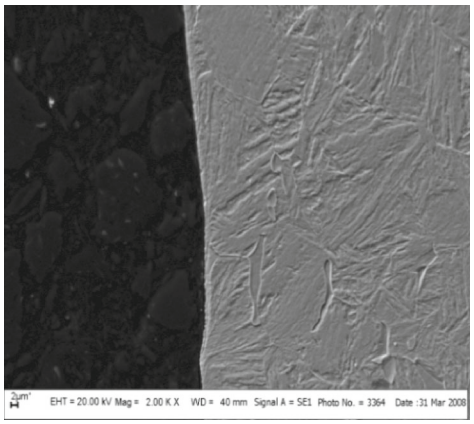

(a) Trend of micro hardness change on subsurface of sample 1 (b) SEM image of metallurgical structure of sample 1

Fig. 11 Trend of micro hardness change on the subsurface of sample 1 and its metallurgical structure

Consequently, both crystal grain strengthening and crystal boundary strengthening take place in hardening the subsurface. Materials in the sample have a phase transition temperature of 605 °C with the cutting zone being at an average temperature of about 250 °C, and the area subject to phase transition is extremely limited even if the temperature rises in local areas.

Figure 12a, b is the trend of micro hardness change of subsurface of sample 2 and its SEM image of metallurgical structure. Sample 2 was machined with feed rate $f = 0.1$ mm/tooth and cutting speed $v = 35$ m/min. The sudden change of the micro-hardness occurred at the place of 0.03 mm underneath the surface. The corresponding micro hardness of the machined surface is 323 HV. It shows that the depth of the hardened layer of sample 2 is about 0.027 mm and that its degree of machining hardness is about 6% under the above conditions. The depth of amorphous layer is 3 μm. The streamline distribution becomes more evident in the subsurface structure. Due to a higher cutting speed and shorter duration of compression and friction on the machined surface, the crystal grain dislocation reduces and the crystal boundary change is limited so that the effects of crystal grain strengthening and crystal boundary strengthening are less than those of sample 1 and its hardening layer is shallower as well.

The trend of micro hardness change on subsurface of sample 3 and its SEM image of metallurgical structure can be seen in Fig. 13a, b with feed rate $f = 0.1$ mm/tooth and cutting speed $v = 40$ m/min. According to the profile of the trend, the micro hardness of the sample 3 has obvious changes down to a depth of 0.022 mm, and the degree of machining hardness is about 4.2%. The depth of amorphous layer declines to 1 μm. Due to alleviated compression and friction of the milling edge on the machining surface, the extent of crystal grain dislocation and crystal boundary change further weakened; the effects of crystal grain strengthening and crystal boundary strengthening are limited; the work hardening layer is shallower.

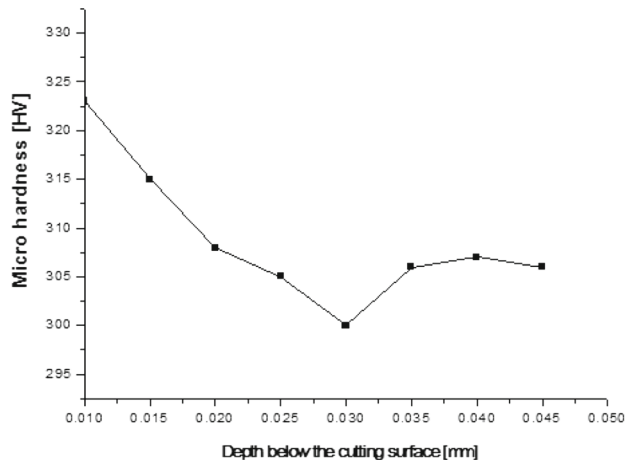

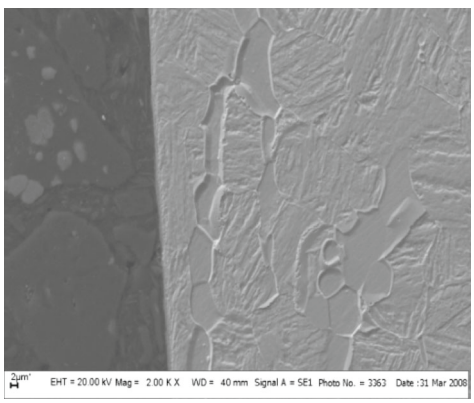

(a) Trend of micro hardness change on subsurface of sample 2 (b) SEM image of metallurgical structure of sample 2

Fig. 12 Trend of micro hardness change on subsurface of sample 2 and its metallurgical structure

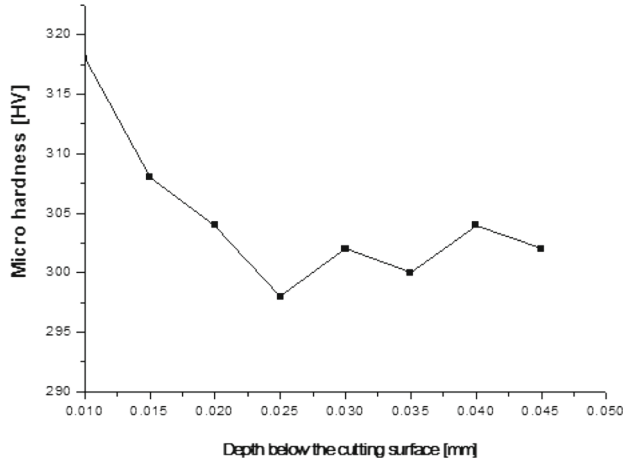

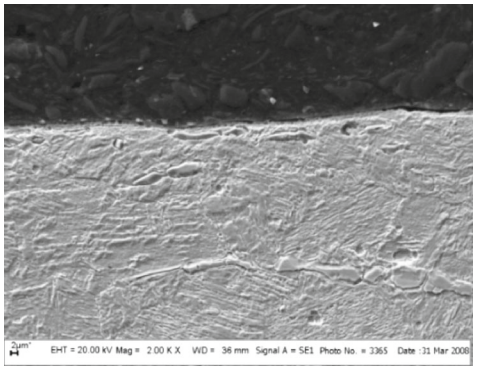

(a) Trend of micro hardness change on subsurface of sample 3 (b) SEM image of metallurgical structure of sample 3

Fig. 13 Trend of micro hardness change on subsurface of sample 3 and its metallurgical structure

When the cutting speed increased to 50 m/min, the trend of micro hardness change on subsurface in sample 4 and its metallurgical structure are respectively shown in Fig. 14a, b. The depth of the hardened layer increased to approximately 0.032 mm with the degree of machining hardness being 6.2%. As the milling speed increased, the cutting region had an average temperature of about 300 °C and the materials in the first milling zone have higher strains and stresses. On the one hand, the depth of amorphous layer increased to 3 μm. On the other hand, the density of dislocation of the crystal grains and the deformation of crystal boundary in the plastically deformed layer on the machined surface increased, thereby enhancing the effects of crystal grain strengthening and crystal boundary strengthening and deepening the workpiece hardening layer.

The experiments mentioned above were conducted at a feeding rate of f = 0.01 mm/tooth. Thereafter, experiments were further conducted at a feeding rate of f = 0.15 mm/tooth, 0.20 mm/z, and 0.25 mm/tooth. The relationships among milling speed, the depth of workpiece hardening, and milling temperature are shown in Fig. 15, with the relationships among milling speed, the degree of work hardening, and milling temperature shown in Fig. 16.

The results show that the depth of hardening layer hc = f(v) and hardening degree N = f(v) have an extreme property of minimum value at the optimal milling zone. As to different feed rates, a higher milling speed leads to a gradual decrease in the hardening depth and the hardening degree. Minimum hardening depth and degree occurring at the optimal milling temperature bring the optimal tool wear.

5.6 The coupling equation of milling parameters

Combined with Eq. 5, the optimum cutting temperature of the minimum tool wear and minimum degree of work hardening

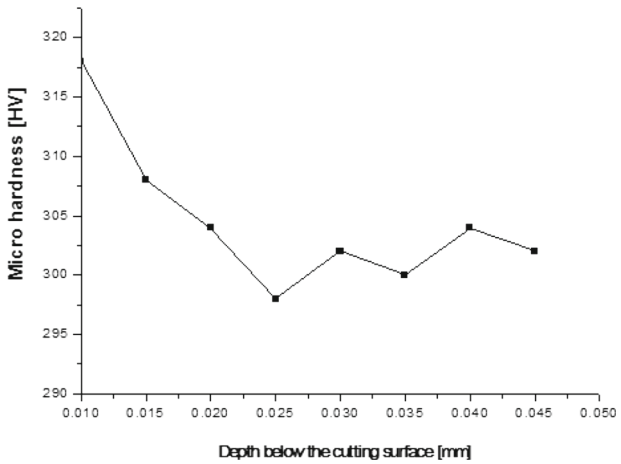

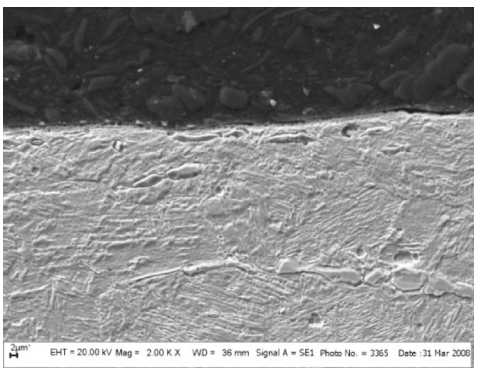

(a) Trend of micro hardness change on subsurface of sample 4 (b) SEM image of metallurgical structure of sample 4

Fig. 14 Trend of micro hardness change on subsurface of sample 4 and its metallurgical structure

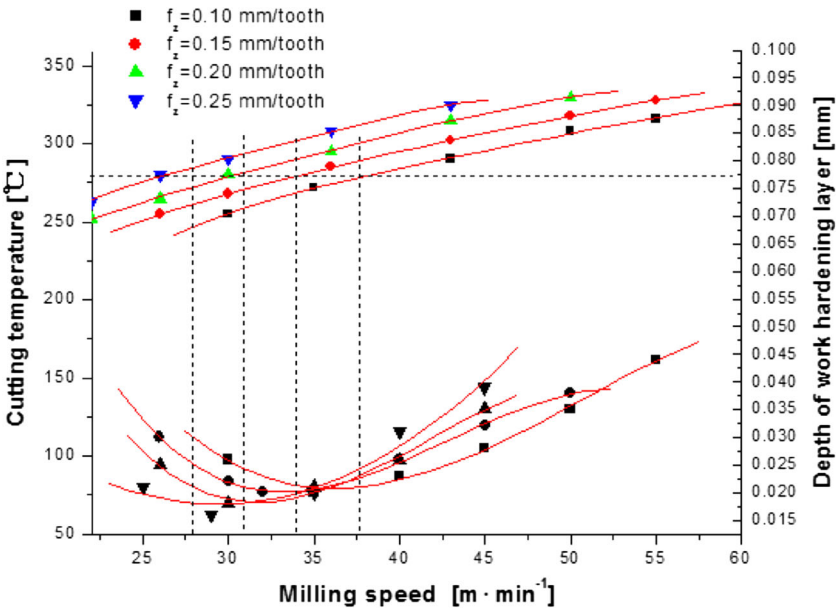

Fig. 15 The relationships of milling speed on the depth of workpiece hardening layer and milling temperature

is 275°C, and the coupling equation of cutting parameters and optimizing cutting temperature is expressed as,

$$a_e^{0.1722} a_p^{0.0007} f^{0.0580} v^{0.3950} = 4.76 \quad (15)$$

Equation 15 shows the relations coupling relationship among radial cutting depth, axial cutting depth, feed rate, and cutting speed at the optimum cutting temperature. The cutting parameters of the cutting process are set up by this equation, which can make the cutting area reach the optimal cutting temperature quickly. Equation 15 is also the basis of cutting parameters adjustment or control in the machining process.

6 Conclusion

Taking the cutting quality, production efficiency, and machining cost as a set of goals, the optimization of cutting parameters was studied by many researchers. However, the relationship among cutting parameters based on the minimum tool wear and work hardening capacity were seldom considered. Many existing researches have established the prediction model of the tool wear value with other optimization models mentioned above to get the optimal cutting parameters. These parameters, however, are not able to ensure the minimum tool wear. If the prediction model of the tool wear value mentioned above is replaced with the coupling model of cutting parameters

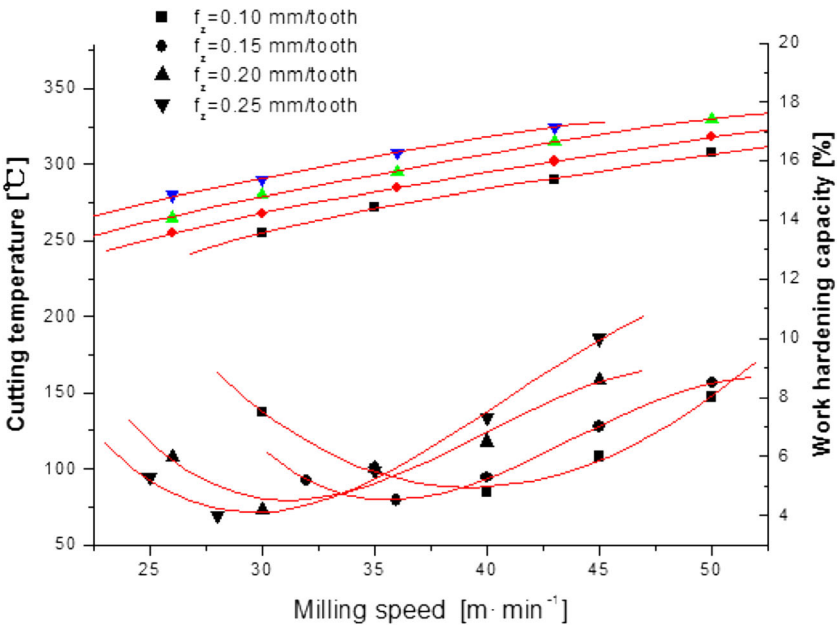

Fig. 16 The relationships of milling speed on the degree of workpiece hardening and milling temperature

proposed in this paper, the optimal goals and ensuring the minimum tool wear can be achieved at the same time.

The paper puts forward the modeling cutting parameters coupling equation based on optimal cutting temperature. The equation can be used as constraint conditions of optimization model. Therefore, it will solve cutting parameter problems to meet the customers' demands with minimum tool wear. The research works are summarized as follows:

1. The optimal cutting temperature is 275 °C when the stainless precipitation-hardening workpiece in this experiment was machined with the cemented carbide YT5 tool.
2. The existence of minimum cutter wear was explored through cutting tests. Based on the measurement of the ratio of the cutter wear of the 1000 cm^2 cutting area, the relationship between the optimal cutting parameters and the optimal machining temperature was found.
3. The depth of work hardening layer and work hardening degree were discussed, with the results showing that they had minimum values at the same temperature corresponding to the minimum tool wear value.
4. The wear mechanisms in cutting process were analyzed. The chemical composition on the cutter wear area was obtained by energy spectrum analyzer, and its wear patterns and their causes in different cutting parameters were analyzed.
5. The optimization equations between the feed rate and the cutter wear value per 1000 cm^2 cutting area and between feed rate and cutting speed were derived from constant cutting speeds, width of cut, and depth of cut.
6. The coupling equation by which to denote the relationships among the cutting parameters was obtained. As a result, any one of the four parameters such as cutting speed, feed rate, width of cut, and depth of cut can be obtained by solving the equation and it will meet the requirements of minimal tool wear in machining process.

The rules between cutting temperature and the wear of cutting tool were investigated, an indication that there was a cutting temperature corresponding to the minimum tool wear value. So, the study provided a theoretical basis for the correct use of cutting fluid or other cooling media and optimal temperature control in the cutting process.

Acknowledgments The authors would like to acknowledge the financial support from the Fujian Science and Technology Flatform Project (grant No. 2016BJ001) and the Science & Technology Innovation Project of Fujian Province (grant No. 2016H2003).

References

1. Khamel S, Ouelaa N, Bouacha K (2012) Analysis and prediction of tool wear, surface roughness and cutting forces in hard turning with CBN tool. J Mech Sci Technol 26(11):3605. doi:10.1007/s12206-012-0853-1
2. Bhushan RK (2013) Optimization of cutting parameters for minimizing power consumption and maximizing tool life during machining of Al alloy SiC particle composites. J Clean Prod 39:242–254
3. Camposeco-Negrete C (2013) Optimization of cutting parameters for minimizing energy consumption in turning of AISI 6061 T6 using Taguchi methodology and ANOVA. J Clean Prod 53(16):195–203
4. Yildiz AR (2013) Optimization of cutting parameters in multi-pass turning using artificial bee colony-based approach. Inf Sci 220(1):399–407
5. Liu ZY, GuoY B, Sealy MP, Liu ZQ (2016) Energy consumption and process sustainability of hard milling with tool wear progression. J Mater Process Technol 229:305–312
6. Yusup N, Zain AM, Hashim SZM (2012) Overview of PSO for optimizing process parameters of machining. Procedia Eng 29:914–923
7. Pervaiz S, Deiab I, Darras B (2013) Power consumption and tool wear assessment when machining titanium alloys. Int J Precis Eng Manuf 14(6):925–936
8. Bhattacharya A, Das S, Majumder P, Batish A (2009) Estimating the effect of cutting parameters on surface finish and power consumption during high speed machining of AISI 1045 steel using Taguchi design and ANOVA. Prod Eng 3:31. doi:10.1007/s11740 -008-0132-2
9. Moussaoui K, Monies F, Mousseigne M, Gilles P, Rubio W (2015) Balancing the transverse cutting force during inclined milling and effect on tool wear: application to Ti6Al4V. Int J Adv Manuf Technol 82(2):1859. doi:10.1007/s00170-015-7518-z
10. Lawal SA, Choudhury IA, Nukman Y (2015) Experimental evaluation and optimization of flank wear during turning of AISI 4340 steel with coated carbide inserts using different cutting fluids. J Inst Eng Aerosp Eng 96(1):21–28
11. Muthusamy Y, Kadirgamal K, Rahman MM, Ramasamy D, Sharma KV (2015) Wear analysis when machining AISI 304 with ethylene glycol /TIO2 nanoparticle-based coolant. Int J Adv Manuf Technol 82:327. doi:10.1007/ s00170-015-7360-3
12. Chetan, Narasimhulu A, Ghosh S, Rao PV (2015) Study of tool wear mechanisms and mathematical modeling of flank wear during machining of Ti alloy (Ti6Al4V). J Inst Eng 96(3):279–285
13. Park KH, Kwon P, Kim D (2012) Wear characteristic on BAM coated carbide tool in drilling of composite /titanium stack. Int J Precis Eng Manuf 13(7):1073. doi:10.1007/s12541-012-0140-1
14. Cui X, Zhao B, Jiao F, Zheng J (2016) Chip formation and its effects on cutting force, tool temperature, tool stress, and cutting edge wear in high- and ultra-high-speed milling. Int J Adv Manuf Technol 58:885. doi:10.1007/s00170-015-7539-7
15. Bugdayci B, Lazoglu I (2015) Temperature and wear analysis in milling of aerospace grade aluminum alloy Al-7050. Prod Eng 9(4): 487. doi:10.1007/s11740-015-0623-x
16. Lin H, Wang C, Yuan Y (2015) Tool wear in Ti-6Al-4V alloy turning under oils on water cooling comparing with cryogenic air mixed with minimal quantity lubrication. Int J Adv Manuf Technol 81(1):1–15
17. Neto RRI, Scalon VL, Fiocchi AA, Sanchez LEA (2016) Indirect cooling of the cutting tool with a pumped two-phase system in turning of AISI 1045 steel. Int J Adv Manuf Technol 87(9):2485. doi:10.1007/s00170-016-8620-6
18. Luo M, Wang J, Wu B et al (2016) Effects of cutting parameters on tool insert wear in end milling of titanium alloy Ti6Al4V. Chin J Mech Eng:1–7
19. Hao ZP, Fan YH, Lin JQ, Yu ZX (2015) Wear characteristics and wear control method of PVD-coated carbide tool in turning inconel 718. Int J Adv Manuf Technol 78(5):1329. doi:10.1007/s00170-014-6752-0
20. Sheng J (2015) A modeling method for turning parameters coupling based on minimum cutting tool wear. Int J Adv Manuf Technol 76(1):705. doi:10.1007/s00170-014-6318-1